EPJ Web of Conferences **95**, 03017 (2015)
DOI: 10.1051/epjconf/20159503017

Results from the AMS02 experiment on the International Space Station

Marco Incagli[1,a], on behalf of the AMS Collaboration

[1] *Istituto Nazionale di Fisca Nucleare (INFN) - Pisa*

Abstract. AMS02 experiment has collected data on Cosmic Rays for three years on the International Space Station, since its installation on May, 19 2011. The fluxes of electrons, positrons and protons, together with the results on Boron and Carbon ratio, will be discussed, as well as their implication in terms of Cosmic Ray propagation and in terms of limits on the existence of Dark Matter in the electroweak energy range.

1 Introduction

The AMS-02 experiment is a multi-purpose particle detector experiment mounted on the International Space Station (ISS). It has been gathering data since May 2011 detecting and identifying cosmic-ray electrons, positrons, protons, anti-protons, heavy nuclei up to Zinc (Z=30) and photons. Recently, first results on the measurement of the cosmic-ray positron fraction and on the absolute fluxes of electrons and positrons have been published [1–4] and will be reviewed in this presentation. The positron fraction has been measured with unprecedented accuracy up to 500 GeV and emphasizes the need of a primary source of positrons to explain the rise of the positron fraction at high energies.

Investigation of such a source must include a description of the individual fluxes of cosmic ray (CR) electrons and positrons, but also protons and Helium, which are the most abundant component of the global CR flux. At the same time, understanding the propagation of CR in the galaxy is fundamental to establish the behaviour of the standard secondary production. Particularly sensitive to this is the ratio B/C, being Boron an almost pure product of the interaction of primary nuclei, mostly Carbon, with the Interstellar Medium (ISM).

In section 2 the AMS02 Detector and its capability of discriminating positrons from protons as well as positive from negative charges is described. Section 3 reports the spectrum of electrons and positrons, while section 4 is dedicated to hadron physics: protons, Helium and B/C.

2 The AMS-02 Detector

The AMS-02 detector consists of nine planes of precision silicon tracker, with 6 planes of the inner tracker located inside the bore of a permanent magnet, a transition radiation detector (TRD), four planes of time of flight counters (TOF), an array of anti-coincidence counters (ACC) surrounding the inner tracker, a ring imaging Cherenkov detector (RICH) and an electromagnetic calorimeter (ECAL).

[a] e-mail: marco.incagli@pi.infn.it

For a detailed description of the detector see [1] and references therein. Here only the parameters relevant for the different analyses will be described. In particular, the TRD and ECAL capabilities of discriminating positrons from protons, the tracker capability in determining the charge sign and the charge (Z) resolution of the various subdetectors will be discussed in the next sub-sections.

2.1 ep rejection

There are three main detectors which allow for a significant reduction of the tremendous proton background in the positron and electron samples, the so called *ep rejection*. These are the TRD, the ECAL standalone and the ECAL in conjuction with the tracker through the comparison of the independent measurements of Energy and Momentum (E/p ratio).

2.1.1 ep rejection with TRD

The TRD measures the transition radiation which is emitted by relativistic particles when crossing boundaries between materials having a different dielectric constant [5].

In order to differentiate between electrons and protons, up to 20 signals from TRD layers are combined in a TRD estimator formed from the ratio of the log-likelihood probability of the $e^{\pm}$ hypothesis to that of the p hypothesis. The probabilities are calculated from the probability density function $f(s)$ of the TRD signals s for each species as $P_x = \sqrt[n]{\Pi_i f_x(s_i)}$, with $x = e^{\pm}, p$. The resulting rejection power for a 90% efficiency for $e^{\pm}$ measured in orbit is shown in fig.1 and it exceeds 10^3 for most of the momentum range. Note that the proton rejection power can be readily improved by tightening the selection criteria with reduced $e^{\pm}$ efficiency, as shown by the line at 1 TeV in the same figure.

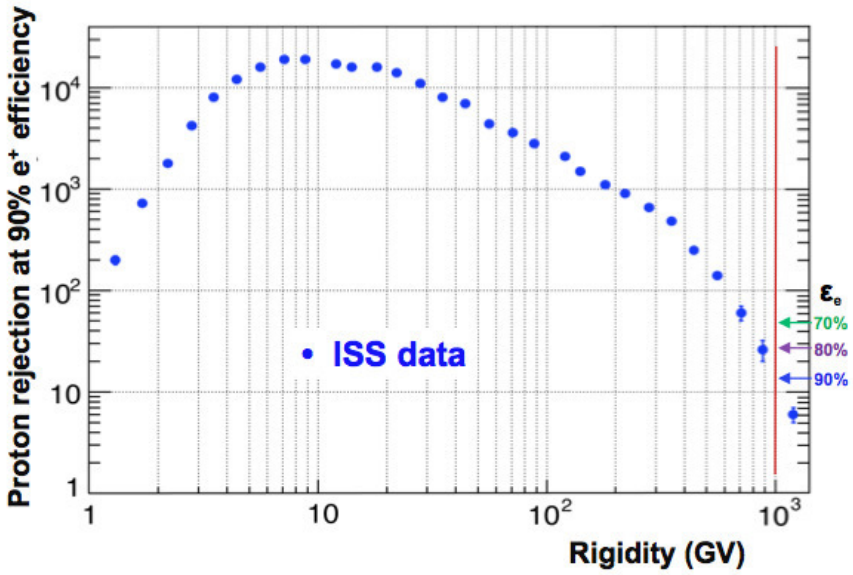

Figure 1. Proton rejection power at 90% signal efficiency with TRD detector.

2.1.2 ep rejection with ECAL

The discrimination between electrons and protons in ECAL is based on the different characteristics of electromagnetic and hadronic showers. For this reason, ECAL is segmented in cells of 9×9 mm^2, corresponding to 0.94 X_0 (radiation lengths) in the longitudinal direction and to 0.5 R_M (Moliére radii) in the transveral one.

A set of variables which describe the shower development, like the transversal width, the number of hits, the fraction of energy per layer, etc., are combined together by means of a multivariate analysis in order to provide the ECAL estimator shown in fig.2.a . The statistical technique used for combining the input variables into a single estimator is the Boosted Decision Tree (BDT) [6].

In addition, leptons and hadrons can be discriminated by the ratio E/p, where E is the energy measured by the ECAL and p the momentum measured by the tracker. In fact hadron showers tend to have a larger leakage than the electromagnetic ones, and therefore a smaller value of E/p.

By combining a cut on the ECAL BDT at 90% efficiency on the signal with a cut on $E/p > 0.75$, the ep rejection of fig.2.b is obtained. When combined with the TRD rejection of fig.1, the required ep rejection of $10^5 - 10^6$ is reached.

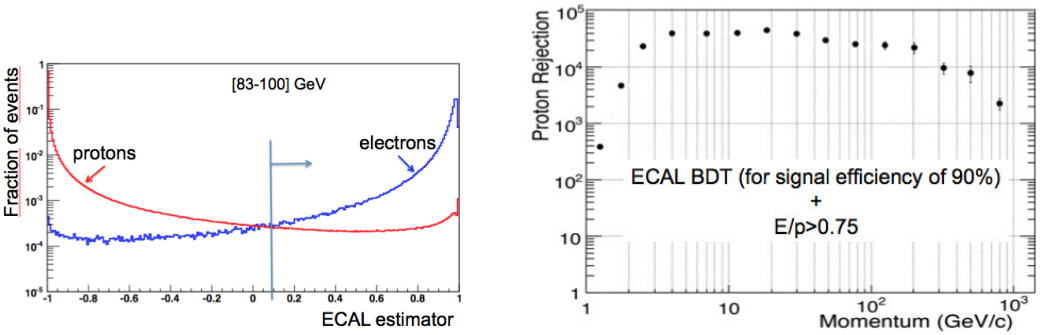

(a) (b)

Figure 2. a) ECAL estimator for 100 GeV electrons and protons selected by TRD and tracker sign. b) Proton rejection for a combined cut on ECAL estimator and on E/p>0.75 (energy-momentum matching).

2.2 Charge Confusion

A fraction of charged events, depending on the particle momentum, are wrongly reconstructed as positive tracks being negative and viceversa. There are two effects which can induce this charge confusion (CC). The first one is the finite tracker resolution in measuring the rigidity R of the track, shown in fig.3.a. This effect, called *spillover*, is parametrized and it turns out to be negligible at 300 GeV, while at E=1 TeV it is 2%.

The second effect is the production of secondary tracks along the particle path, due to interactions with the $0.6X_0$ of the detector material above ECAL. These secondary tracks create additional hits close to the ones due to the main particle; as a consequence a CC due to *wrong hits association* can be induced. Differently from the *spillover* effect, this one is different for electrons and protons, as the synchroton emission of secondary particles is proportional to the particle mass squared. However it can be quantified by building a *tracker estimator*. very similar to the one used for ECAL. It is built by

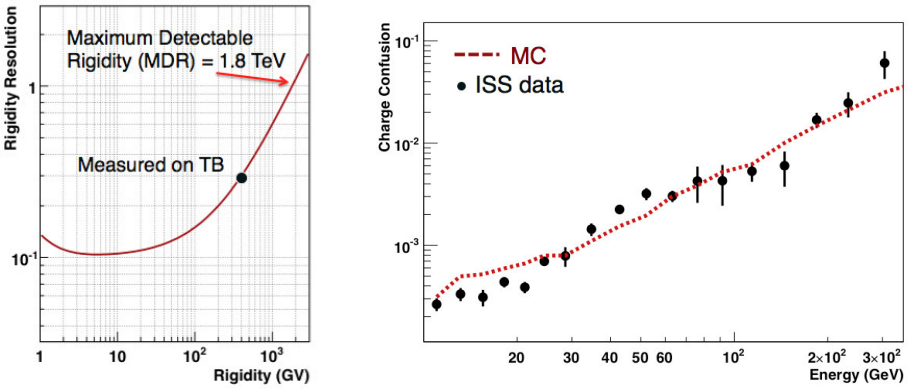

(a) (b)

Figure 3. a) Tracker rigidity resolution on protons. b) Charge Confusion due to wrong hit association.

using a set of input variables which are sensitive to the layer activity: number and distance from the main track of the hits in each tracker plane, χ^2 of the tracker fit, number of hits in TRD, etc. These variables are combined by the BDT technique in a single classifier, which has been tested on Test Beam data, where the correct track sign is known A good agreement of the classifier between data and Montecarlo (MC) is observedm as shown in fig.3.b, which allows us to use MC to determine the fraction of CC events as a function of energy.

2.3 Z reconstruction

The value of the nuclear charge Z of incoming particles is measured, in AMS, by many subsystems. The first tracker layer plane, on the top of the detector, determines the charge by the dE/dx released in the silicon. The same technique, but with different materials, is used in TRD – energy loss in Xe/CO_2 gas mixture – and in the TOF – two layers of plastic scintillators. The RICH, instead, determines Z by the number of photons in the Cherenkov ring. Figure 4 shows the AMS Z-determination power for the different subsystems for charges up to Oxigen.

3 Leptons

3.1 The positron fraction

The positron fraction is determined in ECAL energy intervals. The binning is chosen according to the energy resolution measured at Test Beam: $\Delta E/E = 10.4\%/\sqrt{(E)} \oplus 1.4\%$, where the symbol $\oplus$ indicates the *sum in quadrature* [7].

In every energy bin, the 2-dimensional reference spectra for $e^{\pm}$ and p are fitted to data in the 2 dimensional (*TRD estimator-log(E/p)*) plane. The reference spectra are determined from high statistics, clean electron and proton data samples, selected using ECAL information, and from Montecarlo simulation.

This *template fit* method, with respect to the more standard sequential cut one, has the advantage of using all the signal statistics thus minimizing the statistical error. It can be profitably used in the

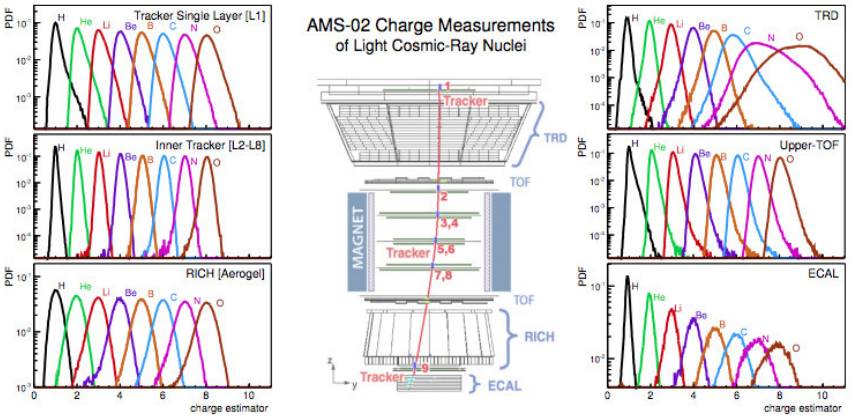

Figure 4. AMS Z reconstruction capability.

AMS context due to the redundancy in the detector which allows for the selection of clean samples of electrons and protons in TRD by using ECAL and viceversa. The systematics introduced by this procedure, as well as all the other sources of systematic errors, is discussed in detail in [1].

The measured positron spectrum is shown in fig.5.a, with a zoom of the high energy part in fig.5.b.

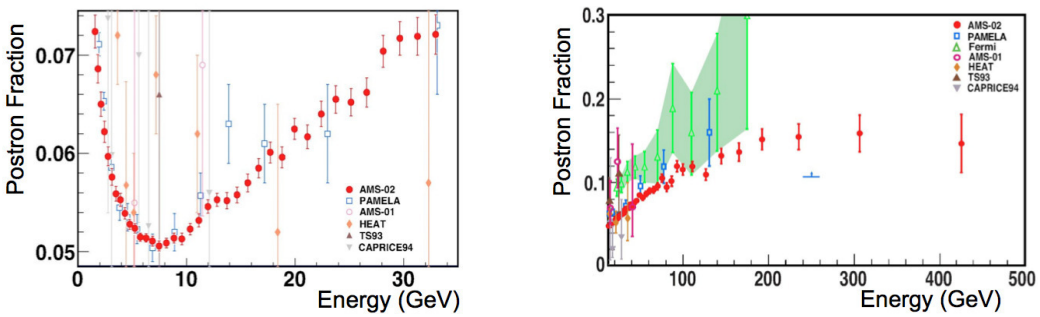

(a) (b)

Figure 5. a) Positron fraction. b) Positron fraction above 20 GeV

The positron fraction is steadily increasing from 10 to 200GeV, then it clearly starts to flatten out. The AMS-02 spectrum has the unique accuracy and energy range to provide accurate information on new phenomena.

3.2 Electron and Positron fluxes

The flux of cosmic ray electrons or positrons $\phi_e^{\pm}$ in energy bins ΔE can be determined as

$$\phi_e^{\pm} = \frac{N_e^{\pm}}{A_{eff} \cdot \epsilon_{trig} \cdot \epsilon_{sel} \cdot T \cdot \Delta E}, \tag{1}$$

with the number of mesured electrons or positrons $N_e^{\pm}$, the effective acceptance A_{eff}, trigger efficiency ϵ_{trig}, selection efficiency ϵ_{sel} and measurement time T.

The width ΔE of the energy bins are chosen sufficiently large with respect to the energy resolution of the ECAL. This minimizes necessary corrections to the fluxes by unfolding. At high energies larger bin sizes ensure sufficient counting statistics in each bin. The number of events $N_e^{\pm}$ in each bin are evaluated as for the positron fraction analysis.

A loose preselection is used to define stable detector operations for the whole data set. Further quality cuts define a high quality data set with excellent and unambiguous event reconstruction. Events are selected by requiring a track in the TRD and in the tracker, a cluster of hits in the ECAL, and a measured velocity $\beta > 0$ in the TOF consistent with a downward-going $Z = 1$ particles; 30 million events pass this selection.

The ECAL estimator and energy-momentum matching are used to further reject protons. The cuts are chosen to reduce the proton background significantly while keeping a high efficiency on signal events. The remaining event samples of electron and positron candidates are fitted with respect to the TRD Estimator by using templates which describe signal and background.

An example of such a fit for a particular energy interval around $E = 100$ GeV is shown in fig.6. Note that the ratio between positron and proton events, originally at the $10^{-4} - 10^{-3}$ level, depending on the energy, is $\simeq 1 : 1$ after the preliminary cuts on ECAL variables and on E/p.

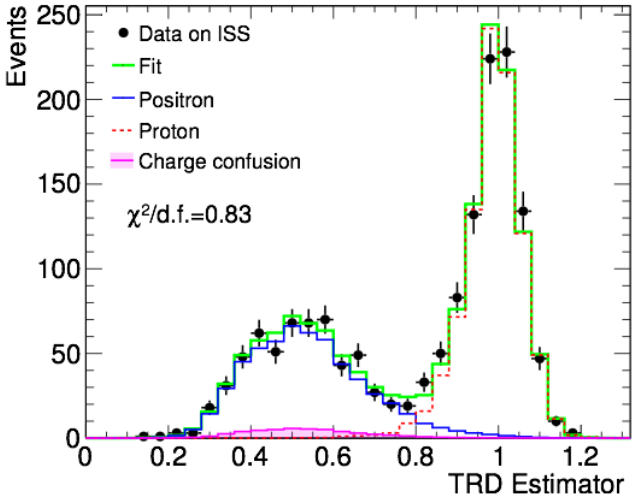

Figure 6. Separation power of the TRD estimator at energy E=100 GeV.

Details on how the geometrical acceptance and efficiencies are evaluated are reported in [2]. The resulting fluxes, when multiplied by the third power of the energy, are shown in fig.7].

The electron flux measurement extends up to 700 GeV. When multiplied by E^3, it is rising up to 10 GeV and it appears to be on a smooth, slowly falling curve above. The measurement is in good agreement with the previous data reported by the PAMELA and HEAT experiments. The differences at low energies can be attributed to the effect of solar modulation.

The positron flux measurement extends up to 500 GeV. When multiplied by E^3, it is rising up to 10 GeV, from 10 to 35 GeV the spectrum is flat and above 35 GeV rises again. The spectral index

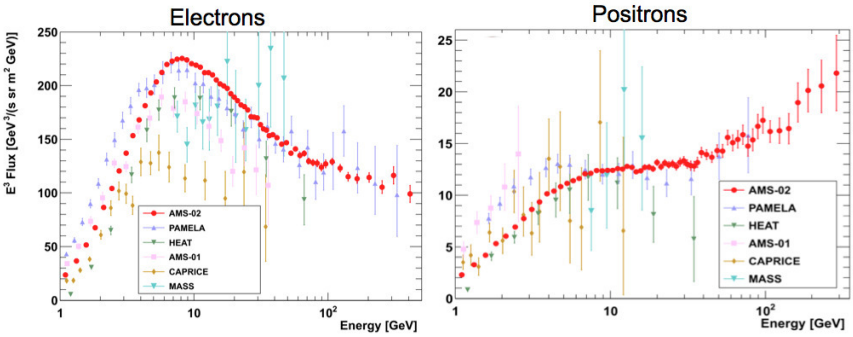

Figure 7. Total flux multiplied by E^3 for electrons (left) and positrons (right).

and its dependence on energy is clearly different from the electron spectrum, and it has the intriguing feature of an index break at 35 GeV.

The total electron flux, intended as the sum of electrons plus positrons, can also be measured by AMS. In this case, the effect of charge confusion is not relevant, therefore the quality cuts applied to select good tracks can be realeased, increasing the efficiency of the analysis. The spectrum can thus be extended up to 1000 GeV (see [3]). The total electron flux, multiplied by E^3, is shown in fig.8. The spectrum doesn't show and evidence of structures and the spectral index seems to be constant above 50 GeV, differently from what observed by other experiments. We have verified that the all electron spectrum is compatible with the sum of the positron and electron spectra, in spite of the fact that the two analyses are completely independent and use different procedures.

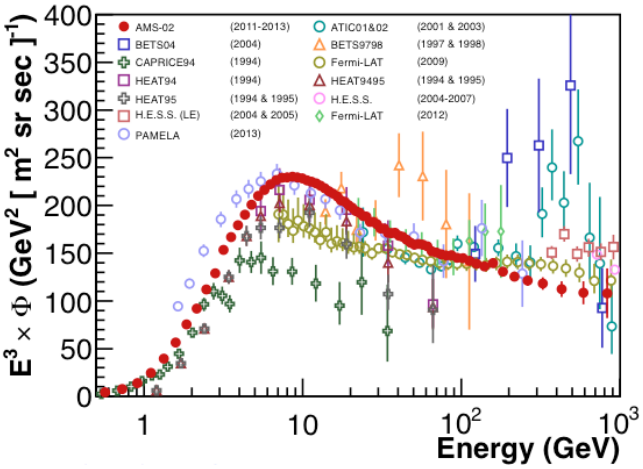

Figure 8. All electron flux multiplied by E^3.

4 Hadron physics

Hadrons are the most abundant particles within the cosmic ray flux; they contribute to 99% of the observed flux of CR.

The general formula to determine their flux is the same as the one for electrons (eq.1). The main difference is that the flux is measured as a function of the tracker rigidity, since dimensions and weight forbid the usage of hadron calorimetry in space. The tracker reaches its Maximum Detectable Rigidity (MDR), defined as the rigidity at which the relative error $\delta R/R$ is 100%, at $R = 2.0$ TeV for protons and at $R = 3.2$ TeV for Helium. At these rigidities, the bin to bin migration is not negligible, therefore an unfolding procedure is required. A preliminary plot of the measured fluxes, to be confirmed by published papers, is shown in fig.9. Details on the selection, on the flux determination and on the unfolding procedure, as well as a discussion of the comparison with previous data at high energies, can be found in [10].

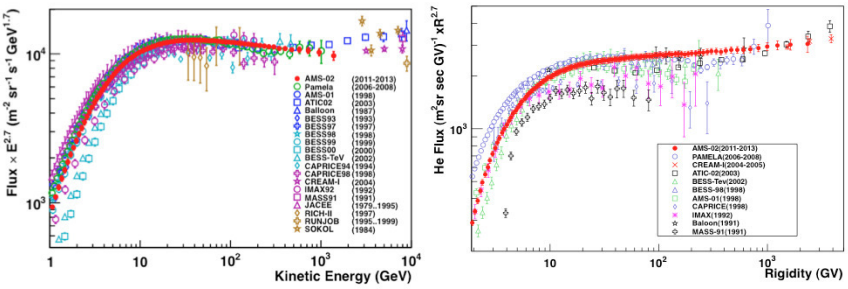

Figure 9. a) Proton flux, multiplied by $E_{kin}^{2.7}$ in the kinetic energy interval [1-1800] GeV. Note that this unit has been used, instead of rigidity, for comparison with older results, in particular in the low (<10 GeV) energy part. b) Helium flux, multiplied by $R^{2.7}$ in the rigidity interval [2-3000] GeV.

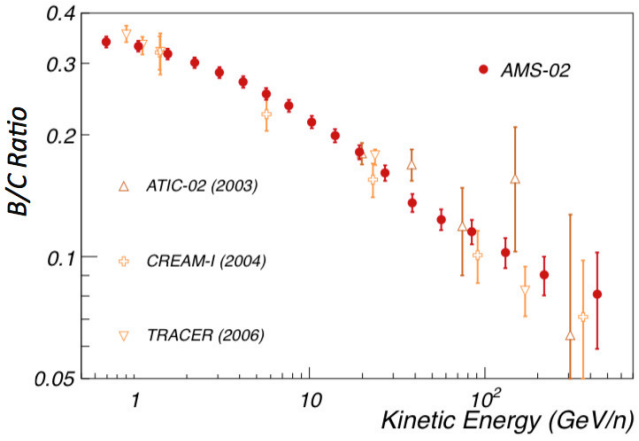

Figure 10. B/C ratio in the kinetic energy interval [0.5,670] GeV/n.

4.1 B/C ratio

The excellent AMS ability in determining the Z charge of nuclei, together with its redundancy in this measurement (see fig.4), allow for the measurement with high precision and in a large energy range of the flux of nuclei above Helium.

Of particular importance is the determination of the fraction of secondary nuclei, i.e. elements which are produced by the interaction of the primary ones with the ISM. A typical example is the Boron (Z=5), which is mostly produced by Carbon (Z=6) interaction with ISM. The ratio B/C, as a function of the rigidity, or kinetic energy, of the particles, provides information on the cosmic ray diffusion properties within the galaxy.

The AMS meaurement is shown in fig.10. A discussion of the possible change of slope in the ratio around $R = 30$ GeV is in [10].

5 Conclusions

Data recorded in the first two years of mission by the AMS experiment have been analyzed and the absolute spectra of protons, Helium, electrons and positrons measured, together with the positron fraction and the B/C ratio. All there results show the precision and the large energy range covered by AMS. Even more, it shows that with a single detector many different channels can be determined at the same time, thus strongly constraining the models of Cosmic Rays propagation in the galaxy and, possibly, models of new physics, both of astrophysical and of particle physics origin.

Acknowledgements

This work has been supported by acknowledged person and institutions in [1], as well as by the Italian Space Agency under contracts ASI-INFN I/002/13/0 and ASD-C/011/11/1.

References

[1] M. Aguilar *et al.* [AMS Collaboration], "First Result from the Alpha Magnetic Spectrometer on the International Space Station: Precision Measurement of the Positron Fraction in Primary Cosmic Rays of 0.5–350 GeV," Phys. Rev. Lett. **110** (2013) 141102.

[2] M. Aguilar *et al.* [AMS Collaboration], "Electron and Positron Fluxes in Primary Cosmic Rays Measured with the Alpha Magnetic Spectrometer on the International Space Station," Phys. Rev. Lett. **113** (2014) 121102.

[3] M. Aguilar *et al.* [AMS Collaboration], "A Precision Measurement of the $(e^+ + e^-)$ Flux in Primary Cosmic Rays from 0.5 GeV to 1 TeV with the Alpha Magnetic Spectrometer on the International Space Station" submitted to Phys. Rev. Lett. .

[4] L. Accardo *et al.* [AMS Collaboration], "High Statistics Measurement of the Positron Fraction in Primary Cosmic Rays of 0.5–500 GeV with the Alpha Magnetic Spectrometer on the International Space Station," Phys. Rev. Lett. **113** (2014) 121101.

[5] K. Luebelsmeyer *et al*, Nucl. Instrum. Methods Phys. Res., Sect. A 654, 639 (2011)

[6] P.R. Byron *et al*, Nucl.Instrum.Meth. A543 (2005) 577

[7] C. Adloff *et al*, Nucl. Instrum. Methods Phys. Res., Sect. A 714, 147 (2013)

[8] W. Xu, "Precision measurement of positron fraction by AMS-02", these proceedings, Proc. of the 14^{th} ICATPP conference on Astroparticle, Particle, Space Physics, Detector for Physics Applications, September 23–27 (2013), Villa Olmo, Como, Italy, World Scientific

[9] M. Duranti, "Precision measurement of the Electrons plus Positrons Spectrum with AMS", these proceedings, Proc. of the 14^{th} ICATPP conference on Astroparticle, Particle, Space Physics, Detector for Physics Applications, September 23–27 (2013), Villa Olmo, Como, Italy, World Scientific

[10] S. Haino, "Recent results of AMS-02", these proceedings, Proc. of the 14^{th} ICATPP conference on Astroparticle, Particle, Space Physics, Detector for Physics Applications, September 23–27 (2013), Villa Olmo, Como, Italy, World Scientific